

Hot Jupiters, cold kinematics

High phase space densities of host stars reflect an age bias

Alexander J. Mustill¹, Michiel Lambrechts¹, and Melvyn B. Davies^{1,2}

¹ Lund Observatory, Department of Astronomy and Theoretical Physics, Lund University, Box 43, 221 00 Lund, Sweden
e-mail: alex@astro.lu.se

² Centre for Mathematical Sciences, Lund University, Box 118, 221 00 Lund, Sweden

Received XXX; accepted YYY

ABSTRACT

Context. The birth environments of planetary systems are thought to influence planet formation and orbital evolution, through external photoevaporation and stellar flybys. Recent work has claimed observational support for this, in the form of a correlation between the properties of planetary systems and the local Galactic phase space density of the host star. In particular, Hot Jupiters are found overwhelmingly around stars in regions of high phase space density, which may reflect a formation environment with high stellar density.

Aims. We instead investigate whether the high phase space density may have a galactic kinematic origin: Hot Jupiter hosts may be biased towards being young and therefore kinematically cold, because tidal inspiral leads to the destruction of the planets on Gyr timescales, and the velocity dispersion of stars in the Galaxy increases on similar timescales.

Methods. We use 6D positions and kinematics from *Gaia* for the Hot Jupiter hosts and their neighbours, and construct distributions of the phase space density. We investigate correlations between the stars' local phase space density and peculiar velocity.

Results. We find a strong anticorrelation between the phase space density and the host star's peculiar velocity with respect to the Local Standard of Rest. Therefore, most stars in “high-density” regions are kinematically cold, which may be caused by the aforementioned bias towards detecting Hot Jupiters around young stars before the planets' tidal destruction.

Conclusions. We do not find evidence in the data for Hot Jupiter hosts preferentially being in phase space overdensities compared to other stars of similar kinematics, nor therefore for their originating in birth environments of high stellar density.

Key words. Planetary systems — open clusters and associations — Planet–star interactions — Stars: kinematics and dynamics — Galaxy: disc — Solar neighbourhood

1. Introduction

The birth environment of a planetary system—the size and density of the stellar cluster or association where the system forms—is thought to have an impact on the nature of the planetary system. This can occur through external photoevaporation of the protoplanetary disc, and/or through stellar flybys truncating the disc or perturbing formed systems (de La Fuente Marcos & de La Fuente Marcos 1997; Laughlin & Adams 1998; Adams et al. 2006; Malmberg et al. 2007b; Winter et al. 2018; Li et al. 2019, 2020a,b). Direct evidence of the impact of birth environments on planetary system formation is hard to obtain, because of the low number (in absolute terms) of planets found in clusters compared to the field, and the challenges of detecting planets around young stars. Winter et al. (2020, henceforth W20) recently proposed an ingenious way around this, by using the local phase space density—the density of nearby stars in the 6D phase space of Galactic position and velocity—of an exoplanet host star as a proxy for the crowdedness of its birth environment. By assuming that the current density reflects the past density at birth, W20 could look for correlations between this density and the properties of planetary systems.

One of the most significant results from W20 was that the host stars of Hot Jupiters are nearly always in “high-density” regions of phase space. This is naturally explained if the primary migration channel for Hot Jupiters is dynamical excita-

tion through planet–planet scattering and/or Lidov–Kozai cycles, followed by tidal dissipation (Rasio & Ford 1996; Weidenschilling & Marzari 1996; Wu & Murray 2003; Fabrycky & Tremaine 2007). Here, the external dynamical perturbations in a dense birth environment would provide the trigger for this high-eccentricity migration to begin (Malmberg et al. 2007a; Parker & Goodwin 2009; Malmberg et al. 2011; Parker & Quanz 2012; Brucalassi et al. 2016; Rodet et al. 2021). Disc migration offers an alternative channel to produce Hot Jupiters (Lin et al. 1996), which might also be affected by the environment through photoevaporation of the protoplanetary disc (Winter et al. 2018).

This interpretation of W20's finding, though, relies on the assumption that a high local phase space density for a star at the present time reflects a high density of its formation environment. Here we examine this assumption. In Hamiltonian mechanics, Liouville's Theorem indeed states that phase space density is constant along trajectories, implying it would be inherited from a star's formation site. But this does not apply to stars in the Galaxy on Gyr timescales, because the Galactic potential is not time-independent, and the dynamics are not completely collisionless, violating the conditions for Liouville's Theorem to apply. In particular, stellar populations get “heated” with age and increase their velocity dispersion and vertical scale height, through interactions with giant molecular clouds and spiral arms (Spitzer & Schwarzschild 1951; Wielen 1977; De Simone et al. 2004; Nordström et al. 2004). Numerical simulations (Kamdar

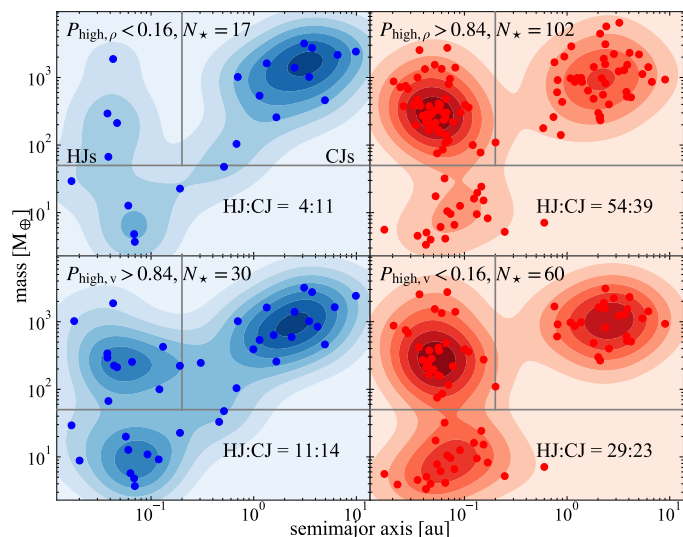


Fig. 1. Semimajor axes and masses of planets whose host stars have masses between 0.7 and $2.0 M_{\odot}$ and ages between 1.0 and 4.5 Gyr. In the top panels they are distinguished by the host stars’ phase space density, in the bottom panel by the host stars’ peculiar velocity. Typically, a low velocity corresponds to a high phase space density and vice versa. We see an abundance of Hot Jupiters in the high-density and the low-velocity populations. Note that stars that cannot be unambiguously assigned to one of the populations are not included, and that some stars have multiple planets.

et al. 2019a,b) find that the imprint of a birth cluster, in comoving conatal pairs and phase space overdensities, largely disappear after ~ 1 Gyr. Hence, it is not clear that the foundational assumption of W20 holds. Instead it is possible that stars’ phase space density reflects coarser features of Galactic structure and kinematics, such as disc heating with age, or the existence of a Galactic thick disc of larger scale height than the thin disc to which the Sun belongs (Gilmore & Reid 1983), rather than the nature of the birth cluster. While noting that Galactic dynamics could play a role in determining the phase space density, W20 interpreted their results in the context of the birth environment hypothesis.

Here we show that, in general, the majority of stars which are currently in “high density” regions of phase space as defined by W20 simply have cold kinematics in the Galactic disc: near-circular orbits and little vertical motion. The “high density” classification thus relates to the lower average age and lesser kinematic heating of the stars, and not to a memory of their birth environment.

2. Methods: Mahalanobis distance and description of the phase space density distribution

We follow W20 in using the Mahalanobis distance (Mahalanobis 1936) in 6D phase space to construct the phase space density. This is essentially a reoriented and stretched Euclidean metric, represented by the quadratic form

$$d_M(\mathbf{x}_1, \mathbf{x}_2; C) = \sqrt{(\mathbf{x}_1 - \mathbf{x}_2)C^{-1}(\mathbf{x}_1 - \mathbf{x}_2)^T}, \quad (1)$$

where \mathbf{x}_1 and \mathbf{x}_2 are two (6D) phase space positions and C is the 6×6 covariance matrix of the whole sample

$$C_{ij} = \langle (x_i - \langle x_i \rangle)(x_j - \langle x_j \rangle) \rangle \quad (2)$$

for $i, j = 1 \dots 6$, where $\langle \dots \rangle$ denotes the mean. It has the advantage of defining a distance in a space whose dimensions have different dynamic ranges and different physical dimensions. However, as it returns a rescaled, dimensionless quantity, its physical interpretation is not obvious. We will therefore relate the density derived from this metric to the host stars’ corresponding physical quantities, especially the peculiar velocity: the star’s velocity with respect to that of a circular orbit in the Galactic plane (the Local Standard of Rest).

We begin by following W20 as closely as possible to ensure a direct comparison with their work. For each target star we:

- Query all objects in *Gaia* Data Release 2 (DR2) or Early Data Release 3 (EDR3) (Gaia Collaboration et al. 2016, 2018, 2021a) within 80 pc of the target. The criterion for inclusion is that the star possess a radial velocity measured by *Gaia* as well as a positive parallax.
- Convert the astrometric, positional and RV information from *Gaia* to a heliocentric Cartesian position and velocity. The distance was obtained by inverting the parallax. A velocity correction from the heliocentric rest frame to the local standard of rest (the velocity of a body on a circular orbit at the Sun’s position in the Galaxy) from Schönrich et al. (2010) was then applied: $(U, V, W)_{\odot} = (11.1, 12.24, 7.25) \text{ km s}^{-1}$.
- Define the Mahalanobis metric on the sample, using the covariance matrix of the positions and velocities of all stars within 80 pc of the target.
- For stars with at least 400 neighbours within 40 pc, randomly choose up to 600 such neighbours. For each of these, as well as the target, find the 20th nearest neighbour by the Mahalanobis distance $d_{M,20}$, and use this to define the local 6D phase space density $\rho_{20} = 20d_{M,20}^{-6}$.
- Normalise ρ_{20} so that the median of the distribution is 1.
- Fit a two-component Gaussian mixture model to the distribution of the logarithm of the rescaled density. Outliers greater than two standard deviations from the mean, or with densities $\rho_{20} > 50$, are clipped before fitting the model.
- Remove systems where a one-component model is a good fit to the density distribution ($p > 0.05$ on a KS test); three systems are so removed.
- Calculate the probability that the target star was drawn from the high-density or the low-density component of the Gaussian mixture model. If $\rho > 50$ assign it to the high density population.

After this, W20 analysed differences between the “high-density” population ($P_{\text{high}} > 0.84$) and the “low-density” population ($P_{\text{high}} < 0.16$). The power of this approach is illustrated in Figure 1, where we show the semimajor axes and eccentricities of known exoplanets¹ whose hosts were cross-matched to *Gaia* EDR3 and whose masses and ages are in the range $0.7 - 2.0 M_{\odot}$ and $1.0 - 4.5$ Gyr (as in W20). As did W20, we see noticeable differences between the distributions of planets orbiting “high-density” and “low-density” hosts. In this paper we focus on the overabundance of Hot Jupiters orbiting the “high-density” hosts: the ratio of Hot to Cold Jupiter hosts is 1.4 for the high-density hosts and only 0.4 for the low-density hosts (in this paper, following W20, we define Hot Jupiters as planets with mass $M > 50 M_{\oplus}$ and semimajor axis $a < 0.2$ au, and Cold Jupiters as planets with mass $M > 50 M_{\oplus}$ and semimajor axis $a > 0.2$ au). As we later argue that tidal effects are likely responsible for the difference between Hot and Cold Jupiters,

¹ From <https://exoplanetarchive.ipac.caltech.edu/index.html>, accessed 2021-03-11.

we also choose a cut between Hot and Cold Jupiters of 0.1 au. This yields similar ratios (for high-density hosts, the Hot to Cold Jupiter ratio is 1.2; for low-density hosts, it is again 0.4). However, in the bottom panels of Figure 1 we show the same sample of planets but with hosts broken down by membership into a high- or low-density component of the distribution of peculiar velocities $|v|$ relative to the Local Standard of Rest, using the same Gaussian Mixture procedure as we used for the densities. Although the difference between the planet populations is not so pronounced as when the hosts are broken down by phase space density, the same trends are seen. This suggests that the stars' peculiar motions are in fact conveying most of the information. With this in mind, we now step back and investigate what the non-dimensionalised, rescaled phase space density is physically telling us.

3. Phase space density and Galactic velocities

We begin by taking the Sun as a case study. W20 identified the Sun as belonging to a phase-space overdensity. This may reflect the Sun's origin in a reasonably large, dense cluster (Adams 2010; Pfalzner et al. 2015). However, we note here that the Sun has a rather low peculiar motion for its age (Wielen et al. 1996; Gonzalez 1999). The colour–magnitude diagram for our sample of Solar neighbours from *Gaia* EDR3 is shown in Figure A.1.

From the Solar neighbours within 40 pc, we have randomly selected 600 and calculated their local phase space density as described above. We show histograms of the phase space density distribution in Figure A.2. In common with the distributions for the neighbourhoods of other target stars, the distribution is poorly fit by a single lognormal. Instead, there is typically a steep cutoff at high density, plus a few high-density outliers often associated with known clusters or moving groups, and a shallower tail towards lower densities. A two- or even higher-component fit is usually superior; in fact, three or more components are often favoured by the Aikake and/or Bayesian Information Criteria, suggesting that the distribution is rather a continuous spectrum than the sum of a high-density and a low-density lognormal. The middle panel of Figure A.2 shows the decomposition into two components. The Sun lies near the peak of the high-density component. Finally, the right panel shows the probability that the Sun belongs to the high-density component, which we calculate to be 0.88. The probability of belonging to the high-density component actually decreases slightly at high densities on account of the breadth of the low-density component. Visual inspection of several distributions showed that this is usually not too extreme a problem; it was helped by clipping the outliers before fitting the Gaussian mixture model as described above. The Sun is found to have a high probability of belonging to the high-density population, as W20 found. In Figure A.3 we show the equivalent Gaussian Mixture models for the velocity distribution; here the Sun belongs to the low-velocity component (the probability it belongs to the high-velocity component is 0.03.)

As the Mahalanobis density is constructed from both spatial and kinematic information, we now ask which of these is most significant. We begin with the velocities, as suggested in Figure 1. Figure 2 shows the local phase space density for neighbours of the Sun and BD+20 2184 (alias Pr0201, a Hot Jupiter host in the Præsepe open cluster, Quinn et al. 2012), as a function of the stars' peculiar velocities. In each case we see a strong correlation: the phase space density is primarily determined by a star's peculiar velocity. “High-density” stars are those with low peculiar velocities, “low-density” stars those with high peculiar velocities. We show in Figure 2 with the background colouring

the approximate velocity ranges corresponding to membership in the Galactic thin disc, thick disc and halo (Bensby et al. 2014). The “low-density” stars appear to be a heterogeneous mix of dynamically hot thin disc stars, thick disc stars, and a handful of halo stars, while the “high-density” stars are lower velocity thin disc stars. A natural interpretation, then is that stars move from the high-density population to the low-density population as they age and are kinematically heated in the disc.

We also see in Figure 2 the Præsepe cluster at $|v| \approx 30 - 40 \text{ km s}^{-1}$, standing out from the field star trend. The field star population is rather smooth; we detrend this in the next section.

In contrast, large-scale spatial structure (*i.e.*, 10s of pc) has little influence on the phase space density. Figure A.4 shows the local phase space density for neighbours of the Sun and BD+20 2184. For the Sun, we see little large-scale spatial structure: the Mahalanobis phase space density of a star is not strongly dependent on its distance to the Sun. For the neighbours of BD+20 2184, the other Præsepe members are clearly identified by the Mahalanobis density measure as a distinct group, attaining densities of $\gtrsim 10^3$ within around 10 pc of the target. However, most of the “high-density” stars as defined by the Gaussian Mixture model are not cluster members: 167 “high-density” stars lie beyond 20 pc of BD+20 2184, and only 74 within 20 pc, those beyond 20 pc having furthermore densities only a little higher than the rest of the field star population, rather than orders of magnitude higher as is the case for the cluster members.

4. Hunting for a trend in the residuals

We now investigate whether there is any correlation of phase space density with the presence of a Hot Jupiter after correcting for the dependence of phase space density on peculiar velocity. Are Hot Jupiter hosts “high-density” when compared to stars of similar kinematics? This could be the case if, for example, stars are born from regions of similar $|v|$ but different densities, and this density difference persists as the stars get heated in the disc.

First we detrend the $\log \rho - \log |v|$ relation. For each of our host stars, we fit a quartic polynomial to $\log \rho$ as a function of $\log |v|$ for each of its sample of neighbours. The example of the Sun is shown in Figure 2. In performing this fit, we exclude densities greater than 50 to avoid the fit being biased by clusters: we wish to fit only field stars. We see in Figure 2 that, although the Sun is a “high-density” host, it lies very close to the fitted trend and is quite unremarkable given its cold kinematics.

We repeat this detrending for each of a sample of Hot Jupiter hosts (planet mass $\geq 50 M_{\oplus}$, planet semimajor axis ≤ 0.2 au, stellar mass $\in [0.7, 2.0] M_{\odot}^2$), as well as for a control sample of cold Jupiter hosts (same criteria except with semimajor axis > 0.2 au). We show the phase space densities as a function of peculiar velocity in the left-hand panel in Figure 3; both populations follow a similar trend to the Solar neighbours in Figure 2. The marginal distributions of both peculiar velocity and phase space density differ significantly ($p = 7.6 \times 10^{-4}$ and $p = 1.1 \times 10^{-4}$ on KS tests), with the Hot Jupiter hosts having lower velocities and higher densities. Our velocity dispersions for the Hot and Cold Jupiter hosts are 37.2 km s^{-1} and 43.3 km s^{-1} respectively, similar to the values obtained by Hamer & Schlaufman (2019)³. In

² This is the same definition of Hot Jupiters as that used by W20, except that we have removed the age constraint: when including the age constraint, the sample was too small to see a significant difference in either ρ or $|v|$.

³ Taking the semi-major axis cut at $a = 0.1$ au, we find 35.3 km s^{-1} and 43.7 km s^{-1} respectively.

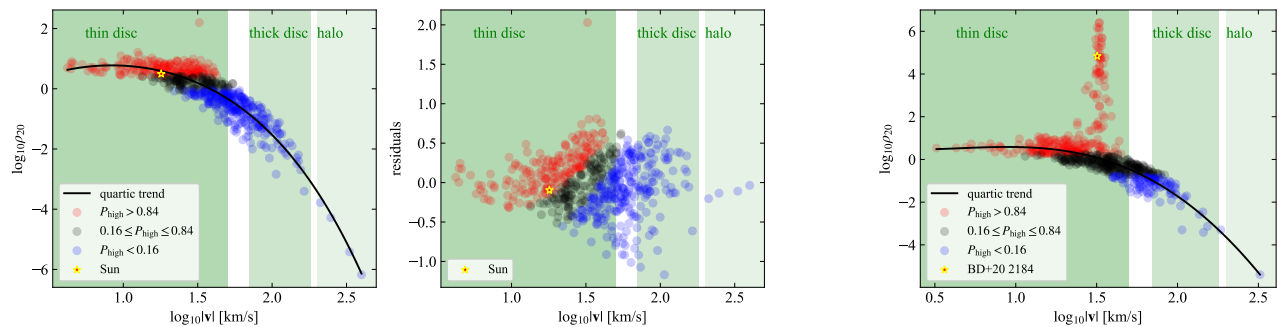


Fig. 2. Left: Local 20th-nearest neighbour phase space density, and probability of membership in the high-density population, for 600 stars within 40 pc of the Sun. We show the fitted quartic trend of the density as a function of peculiar velocity. The outlier at $\rho \sim 150$ is *Gaia* EDR3 3277270538903180160 (LP 533-57, HIP 17766), a Hyades member. Centre: The residuals to the fit, after the trend is removed. Right: The densities and peculiar velocities of 600 neighbours of Pr0201 (BD+20 2184), a Hot Jupiter host in the Præsepe cluster. Pr0201 and other Præsepe members stand out above the trend. Green background shading shows the approximate bounds for membership in the Galactic thin disc, thick disc and halo, from Bensby et al. (2014).

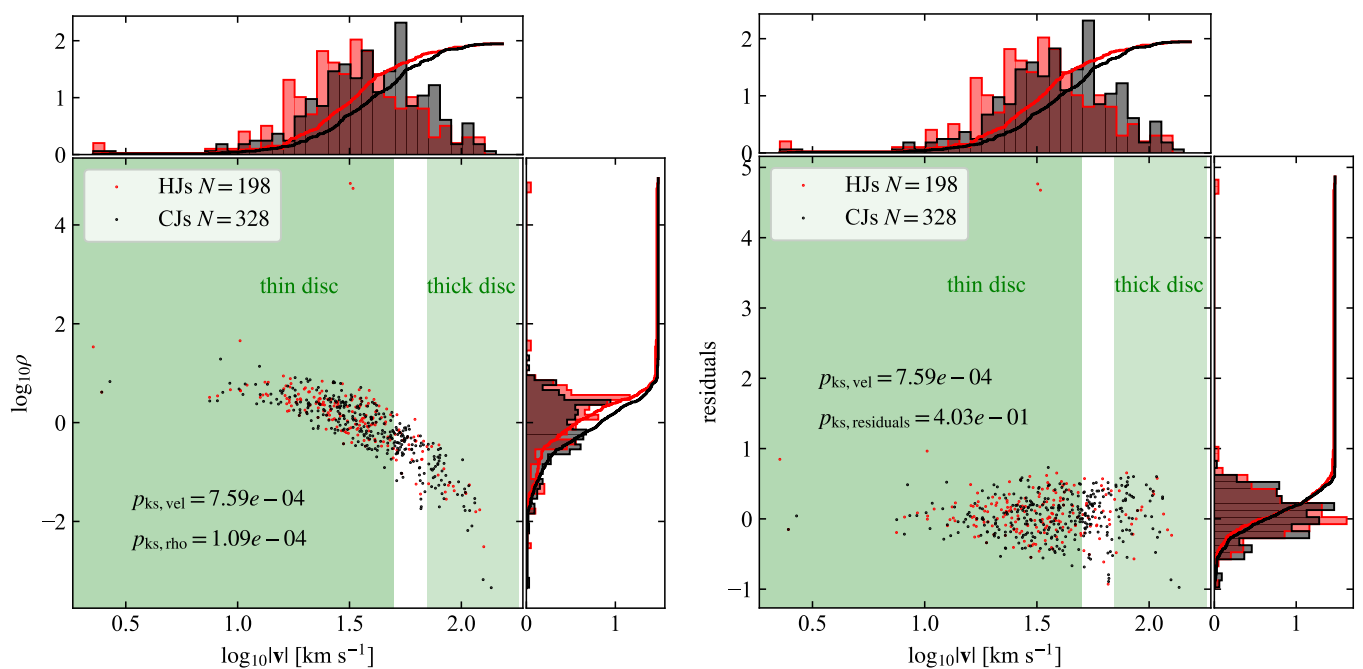


Fig. 3. Left: phase space density versus peculiar velocity for hot Jupiter host stars (‘HJs’) and for cold Jupiter host stars (‘CJs’). Both marginal distributions (top and right sub-panels) are statistically significantly different: the KS-test p -values are shown in the figure. HJ hosts have lower velocity and higher density than CJ hosts. Right: residuals to the detrended phase space density versus peculiar velocity for the same stars. The difference in the distribution of residuals between the Hot and Cold Jupiter populations is not significant ($p_{\text{KS,residuals}} = 0.40$).

the right-hand panel, we show instead the residuals of each host star to its fitted trend. The marginal distributions of these residuals are statistically indistinguishable ($p = 0.40$ on a KS test). Thus, after accounting for the lower velocity dispersion, there is no evidence that the Hot Jupiter hosts are in denser regions of phase space compared to the Cold Jupiter control sample.

In Appendix A.4 we describe an alternative control experiment, in which we compare the hot Jupiter hosts to the 600 randomly-chosen neighbours of the Sun. Again, we find that after accounting for the dependence of the phase space density on velocity, there is no evidence that Hot Jupiter hosts are in regions of high density compared to stars with similar kinematics.

5. Discussion

We have now demonstrated that the main determinant of a star’s 6D phase space density is the magnitude of its peculiar motion, *i.e.*, how much its Galactic orbit deviates from a circular orbit exactly in the Galactic plane. At the present time, and for the past ~ 8 Gyr, stars have been typically born close to the Galactic midplane with a low peculiar velocity, and are heated with age through interactions with matter inhomogeneities in the Galaxy. This heating occurs on a timescale of Gyr: for example, with the good asteroseismic ages derivable from *Kepler* data, Miglio et al. (2021) find that the vertical velocity dispersion for thin disc stars rises from $\approx 10 \text{ km s}^{-1}$ at an age of 1 Gyr to $\approx 20 \text{ km s}^{-1}$ at an age of 10 Gyr. The age–velocity relation for the exoplanet host stars with ages given in the NASA Exoplanet Archive is shown in Fig-

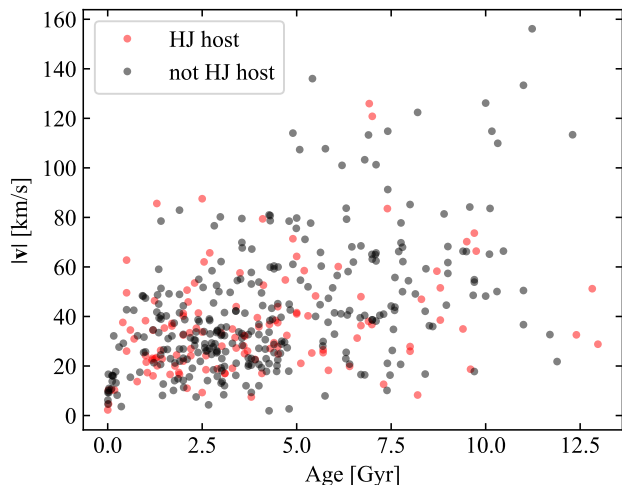


Fig. 4. Age–velocity relation for exoplanet host stars with ages given in the NASA Exoplanet Archive. Stars are divided into Hot Jupiter hosts and non-Hot Jupiter hosts. Error bars on the ages are not shown (indeed, they are not always available) but can easily be several Gyr.

ure 4. We caution that these ages come with large errors, as most exoplanet hosts are main-sequence stars, and are more over not derived homogeneously (see Adibekyan et al. 2021b, for discussion on this). Nonetheless, we do indeed see an increase in the velocity dispersion with age.

This age–velocity relation pertains to the Galactic thin disc. There also exists a chemically distinct and kinematically hotter stellar population, the thick disc, whose stars have a higher velocity dispersion even than thin disc stars of comparable age (Miglio et al. 2021). However, the existence of a clean kinematic separation, and the exact relation of kinematics to abundances and to the early history of the Galaxy are still debated (see, *e.g.*, discussion in Agertz et al. 2021). In principle, a clean kinematic separation between thin and thick discs could be a natural way to interpret the stellar phase space densities, with “high-density” stars being thin disc members and “low-density” stars being thick disc members. However, when we use the rough kinematic classifications from Bensby et al. (2014)—thin disc stars at $|\mathbf{v}| < 50 \text{ km s}^{-1}$ and thick disc stars at $70 \text{ km s}^{-1} \lesssim |\mathbf{v}| \lesssim 180 \text{ km s}^{-1}$ —we see that the “low-density” stars are drawn from both the thick disc and the heated end of the thin disc, with a handful of halo stars as well (see Figure 2). It is likely that the thick disc stars formed on kinematically hot orbits early in the Galaxy’s history due to early mergers and the turbulent nature of the gas disc at early times (Bird et al. 2013; Agertz et al. 2021; Renaud et al. 2021), and they have maintained their higher velocity dispersion (*e.g.*, Miglio et al. 2021) to the present day. This does not affect our argument, since these stars are all old and kinematically hot, and thus have a low phase space density.

As the “high-density” stars are kinematically cold and therefore on average young, and the “low-density” stars are a mix of old thick disc stars and old heated thin disc stars, the stellar age naturally suggests itself as an explanation for the overabundance of Hot Jupiters orbiting “high-density” hosts. Hot Jupiters can spiral in to their host stars under tidal drag (*e.g.*, Jackson et al. 2009; Lévrad et al. 2009; Collier Cameron & Jardine 2018), and if the tidal dissipation is effective enough, the timescale for this is also \lesssim Gyrs, similar to that for kinematic heating of the host star. Hamer & Schlaufman (2019) previously identified that

Hot Jupiter hosts have colder kinematics than Cold Jupiter hosts, with similar values of the velocity dispersions to those we have found, and found that this difference corresponds to tidal decay of Hot Jupiter orbits if the tidal quality factor $Q'_* \lesssim 10^7$. Hot Jupiter hosts, then, are predominantly in high-density regions of phase space because of a bias towards detecting the Hot Jupiters around young stars before their tidal destruction, a bias noted by Collier Cameron & Jardine (2018). A potential confounding factor we have not considered is stellar metallicity, which has a strong influence on the probability of forming a giant planet (Fischer & Valenti 2005). However, in the Solar neighbourhood the age–metallicity relation is rather flat back to ages of around 10 Gyr (Freeman & Bland-Hawthorn 2002; Sahlholdt & Lindgren 2021); for very old stars such as the thick disc, both metallicity and α -element abundance may affect planet formation (Adibekyan et al. 2021a).

We note that we have not shown that there is no impact of birth environment on planetary system architecture, only that the differences found through the phase space method primarily arise as a result of age and that nothing is seen when this confounding factor is removed, at least for the Hot Jupiters. Surveys directly looking at planets in clusters (*e.g.* Rizzuto et al. 2020; Nardiello et al. 2020) could address this, but conclusions may be tentative because of the low yield of discoveries: Brucalassi et al. (2016, 2017) found a Hot Jupiter rate higher in the M67 open cluster than in the field, but this relies on only three Hot Jupiters found in the cluster. There are also other trends found by W20 and subsequent papers (Kruijssen et al. 2020; Chevance et al. 2021; Longmore et al. 2021) that must be explained; we note however that the finding of Chevance et al. (2021) that there is a stronger gradient in planetary radius in multi-planet systems orbiting “low-density” hosts may also be an age effect, as this gradient can result from photoevaporation of the planets’ atmospheres (Owen & Wu 2013) and the older “low-density” stars have more time for this process to proceed. The trend in multiplicity found by Longmore et al. (2021) is harder to explain: they found that low-density hosts have more multiple systems than high-density hosts. This would seem to go against an age dependence (multiplicity should reduce with time), but we note that their good-quality low-density samples had only 5 or 6 stars, and a larger sample would be required to confirm or refute this.

We have followed W20 in using the heterogeneous sample of exoplanets provided by the NASA Exoplanet Archive. Recently, Adibekyan et al. (2021b) used a smaller homogeneous sample to look for differences between the “high-density” and “low-density” populations; the sample was unfortunately too small to see a significant difference. A difference did emerge in a larger sample, although Adibekyan et al. (2021b) noted that the “low-density” hosts are older (with a homogeneous age determination) than the “low-density” hosts. This again underlines the importance of correcting for age. We finish with two further caveats for further studies that may wish to look for trends after the age dependence is removed: first, the differential completeness of *Gaia* across a target star’s neighbourhood should be accounted for (see Figure A.5); and second, coherent structures can arise in velocity space among stars of diverse ages through interactions with matter inhomogeneities in the Galaxy (*e.g.*, De Simone et al. 2004; Antoja et al. 2018; Kushniruk et al. 2020), so phase space overdensities need not reflect a coeval origin in a dense environment.⁴

⁴ While this paper was under review, Kruijssen et al. (2021) submitted a paper linking the phase space densities to such features of Galactic

6. Conclusions

1. Classifying stars according to their local 6D phase space densities, we verify that Hot Jupiter hosts preferentially belong to the population of high phase space density.
2. Phase space density shows an extremely strong anti-correlation with a star's peculiar velocity with respect to the local standard of rest in the Galaxy. The high phase space density of Hot Jupiter hosts is primarily a manifestation of their cold kinematics.
3. After correcting for the dependency of phase space density on peculiar motion, there is no evidence that Hot Jupiter hosts lie in denser regions of phase space than other stars.
4. The observed correlation is likely to arise from the bias towards detecting Hot Jupiters around younger (and therefore kinematically colder) host stars, before the Hot Jupiters are destroyed by tidal orbital decay.

A Jupyter notebook and ancillary files to reproduce these results are available⁵.

Acknowledgements. AJM acknowledges funding from the Swedish Research Council (grant 2017-04945), the Swedish National Space Agency (grant 120/19C), and the Fund of the Walter Gyllenberg Foundation of the Royal Physiographic Society in Lund. This research has made use of the Aurora cluster hosted at LUNARC at Lund University. AJM wishes to thank Ross Church, Sofia Feltzing, Diederik Kruijssen, Steve Longmore, Paul McMillan, Pete Wheatley, Andrew Winter and the anonymous referee for useful comments and discussions. This work has made use of data from the European Space Agency (ESA) mission *Gaia*⁶, processed by the *Gaia* Data Processing and Analysis Consortium (DPAC)⁷. Funding for the DPAC has been provided by national institutions, in particular the institutions participating in the *Gaia* Multilateral Agreement. This research made use of Astropy,⁸ a community-developed core Python package for Astronomy (Astropy Collaboration et al. 2013, 2018). This research made use of NumPy (Harris et al. 2020), SciPy (Virtanen et al. 2020), Matplotlib (Hunter 2007), and Scikit-learn (Pedregosa et al. 2011). This research has made use of the NASA Exoplanet Archive, which is operated by the California Institute of Technology, under contract with the National Aeronautics and Space Administration under the Exoplanet Exploration Program.

References

Adams, F. C. 2010, *ARA&A*, 48, 47
 Adams, F. C., Proszkow, E. M., Fatuzzo, M., & Myers, P. C. 2006, *ApJ*, 641, 504
 Adibekyan, V., Dorn, C., Sousa, S. G., et al. 2021a, *Science*, 374, 330
 Adibekyan, V., Santos, N. C., Demangeon, O. D. S., et al. 2021b, *A&A*, 649, A111
 Agertz, O., Renaud, F., Feltzing, S., et al. 2021, *MNRAS*, 503, 5826
 Antoja, T., Helmi, A., Romero-Gómez, M., et al. 2018, *Nature*, 561, 360
 Astropy Collaboration, Price-Whelan, A. M., SipHocz, B. M., et al. 2018, *AJ*, 156, 123
 Astropy Collaboration, Robitaille, T. P., Tollerud, E. J., et al. 2013, *A&A*, 558, A33
 Bensby, T., Feltzing, S., & Oey, M. S. 2014, *A&A*, 562, A71
 Bird, J. C., Kazantzidis, S., Weinberg, D. H., et al. 2013, *ApJ*, 773, 43
 Brucalassi, A., Koppenhoefer, J., Saglia, R., et al. 2017, *A&A*, 603, A85
 Brucalassi, A., Pasquini, L., Saglia, R., et al. 2016, *A&A*, 592, L1
 Carrasco, J. M., Evans, D. W., Montegriffo, P., et al. 2016, *A&A*, 595, A7
 Casagrande, L. & Vandenberg, D. A. 2018, *MNRAS*, 479, L102
 Cheavance, M., Kruijssen, J. M. D., & Longmore, S. N. 2021, *ApJ*, 910, L19
 Collier Cameron, A. & Jardine, M. 2018, *MNRAS*, 476, 2542
 de La Fuente Marcos, C. & de La Fuente Marcos, R. 1997, *A&A*, 326, L21
 De Simone, R., Wu, X., & Tremaine, S. 2004, *MNRAS*, 350, 627
 Fabrycky, D. & Tremaine, S. 2007, *ApJ*, 669, 1298
 Fischer, D. A. & Valenti, J. 2005, *ApJ*, 622, 1102
 Freeman, K. & Bland-Hawthorn, J. 2002, *ARA&A*, 40, 487

dynamics: the ripples within the Galactic disc generated by matter inhomogeneities such as the bar, arms and satellite galaxies.

⁵ <https://github.com/AJMustill/HJGalaxy>

⁶ <https://www.cosmos.esa.int/gaia>

⁷ <https://www.cosmos.esa.int/web/gaia/dpac/consortium>

⁸ <http://www.astropy.org>

Gaia Collaboration, Brown, A. G. A., Vallenari, A., et al. 2018, *A&A*, 616, A1
 Gaia Collaboration, Brown, A. G. A., Vallenari, A., et al. 2021a, *A&A*, 649, A1
 Gaia Collaboration, Prusti, T., de Bruijne, J. H. J., et al. 2016, *A&A*, 595, A1
 Gaia Collaboration, Smart, R. L., Sarro, L. M., et al. 2021b, *A&A*, 649, A6
 Gilmore, G. & Reid, N. 1983, *MNRAS*, 202, 1025
 Gonzalez, G. 1999, *MNRAS*, 308, 447
 Hamer, J. H. & Schlaufman, K. C. 2019, *AJ*, 158, 190
 Harris, C. R., Millman, K. J., van der Walt, S. J., et al. 2020, *Nature*, 585, 357–362
 Hunter, J. D. 2007, *Computing in Science and Engineering*, 9, 90
 Jackson, B., Barnes, R., & Greenberg, R. 2009, *ApJ*, 698, 1357
 Kamdar, H., Conroy, C., Ting, Y.-S., et al. 2019a, *ApJ*, 884, 173
 Kamdar, H., Conroy, C., Ting, Y.-S., et al. 2019b, *ApJ*, 884, L42
 Kruijssen, J. M. D., Longmore, S. N., & Cheavance, M. 2020, *ApJ*, 905, L18
 Kruijssen, J. M. D., Longmore, S. N., Cheavance, M., et al. 2021, arXiv e-prints, arXiv:2109.06182
 Kushniruk, I., Bensby, T., Feltzing, S., et al. 2020, *A&A*, 638, A154
 Laughlin, G. & Adams, F. C. 1998, *ApJ*, 508, L171
 Levrard, B., Winisdoerffer, C., & Chabrier, G. 2009, *ApJ*, 692, L9
 Li, D., Mustill, A. J., & Davies, M. B. 2019, *MNRAS*, 488, 1366
 Li, D., Mustill, A. J., & Davies, M. B. 2020a, *MNRAS*, 499, 1212
 Li, D., Mustill, A. J., & Davies, M. B. 2020b, *MNRAS*, 496, 1149
 Lin, D. N. C., Bodenheimer, P., & Richardson, D. C. 1996, *Nature*, 380, 606
 Longmore, S. N., Cheavance, M., & Kruijssen, J. M. D. 2021, *ApJ*, 911, L16
 Mahalanobis, P. C. 1936, *Proceedings of the National Institute of Sciences of India*, 2, 49
 Malmberg, D., Davies, M. B., & Chambers, J. E. 2007a, *MNRAS*, 377, L1
 Malmberg, D., Davies, M. B., & Heggie, D. C. 2011, *MNRAS*, 411, 859
 Malmberg, D., de Angeli, F., Davies, M. B., et al. 2007b, *MNRAS*, 378, 1207
 Miglio, A., Chiappini, C., Mackereth, J. T., et al. 2021, *A&A*, 645, A85
 Nardiello, D., Piotto, G., Deleuil, M., et al. 2020, *MNRAS*, 495, 4924
 Nordström, B., Mayor, M., Andersen, J., et al. 2004, *A&A*, 418, 989
 Owen, J. E. & Wu, Y. 2013, *ApJ*, 775, 105
 Parker, R. J. & Goodwin, S. P. 2009, *MNRAS*, 397, 1041
 Parker, R. J. & Quanz, S. P. 2012, *MNRAS*, 419, 2448
 Pedregosa, F., Varoquaux, G., Gramfort, A., et al. 2011, *Journal of Machine Learning Research*, 12, 2825
 Pfalzner, S., Davies, M. B., Gounelle, M., et al. 2015, *Phys. Scr.* 90, 068001
 Quinn, S. N., White, R. J., Latham, D. W., et al. 2012, *ApJ*, 756, L33
 Rasio, F. A. & Ford, E. B. 1996, *Science*, 274, 954
 Renaud, F., Agertz, O., Andersson, E. P., et al. 2021, *MNRAS*, 503, 5868
 Rizzuto, A. C., Newton, E. R., Mann, A. W., et al. 2020, *AJ*, 160, 33
 Rodet, L., Su, Y., & Lai, D. 2021, *ApJ*, 913, 104
 Sahlholdt, C. L. & Lindegren, L. 2021, *MNRAS*, 502, 845
 Schönrich, R., Binney, J., & Dehnen, W. 2010, *MNRAS*, 403, 1829
 Spitzer, Lyman, J. & Schwarzschild, M. 1951, *ApJ*, 114, 385
 Virtanen, P., Gommers, R., Oliphant, T. E., et al. 2020, *Nature Methods*, 17, 261
 Weidenschilling, S. J. & Marzari, F. 1996, *Nature*, 384, 619
 Wielen, R. 1977, *A&A*, 60, 263
 Wielen, R., Fuchs, B., & Dettbarn, C. 1996, *A&A*, 314, 438
 Winter, A. J., Clarke, C. J., Rosotti, G., et al. 2018, *MNRAS*, 478, 2700
 Winter, A. J., Kruijssen, J. M. D., Longmore, S. N., & Cheavance, M. 2020, *Nature*, 586, 528
 Wu, Y. & Murray, N. 2003, *ApJ*, 589, 605

Appendix A: Additional figures

Appendix A.1: Colour–magnitude diagram for Solar neighbours

We show the colour–magnitude diagram for our sample of Solar neighbours in Figure A.1. We have, in keeping with W20, imposed no quality cuts on the *Gaia* data (other than the need for parallax to be positive); however, note that moving from DR2 to EDR3 cleans the CMD considerably, especially of spurious objects below the main sequence. The blob at $M_G \sim 8$, below the main sequence, is discussed in Gaia Collaboration et al. (2021b), who attributed it to a change at $G = 13$ in the window of pixels on the CCD surrounding around the target (Carrasco et al. 2016). In this paper, we work with the EDR3 data.

Appendix A.2: Gaussian mixture model

In Figure A.2 we show the Gaussian mixture model for the Sun and 600 of its neighbours, together with the stars’ probability of belonging to the high-density population. Note that this probability begins to decrease slightly for stars with moderately high densities, on account of the breadth of the low-density distribution. Stars at $\rho > 50$ are assigned $P_{\text{high}} = 1$ to alleviate this. We show the equivalent decomposition in velocities in Figure A.3.

Appendix A.3: Spatial structure

In Figure A.4 we show the phase space density as a function of distance to the target star, for 600 neighbours of the Sun and of the Præsepe member BD+20 2184. There is little structure seen among the neighbours of the Sun, although there may be a weak trend from 25 to 40 pc; this disappears if we restrict attention to stars with an absolute magnitude $M_G \leq 8$ and may reflect the decreasing completeness of *Gaia* with distance. For BD+20 2184, fellow cluster members stand out at high density close to the target.

We show in Figure A.5 the differential completeness of the *Gaia* EDR3 RV catalogue across a sphere of 80 pc centred on BD+20 2184. Looking at the top panels, we see that the 3D spatial density of stars in the RV catalogue falls by a factor of three between the near side of the sphere and the far side of the sphere. This seems not to induce a strong bias in the spatial density as a function of distance from BD+20 2184 itself, shown in the bottom right panel: the Præsepe cluster clearly stands out as a significant spatial overdensity, beyond which the density is constant. Nevertheless, the potential for the differential completeness to induce a bias should be borne in mind as a potential confounding factor once the main velocity dependence of the phase space density is accounted for.

Appendix A.4: Alternative detrending comparison

In the main body of the paper (§4), we showed that the phase space density residuals, after the velocity trend is removed, are identical for the Hot Jupiter hosts and for the Cold Jupiter hosts. This implicitly puts all of the phase space densities on the same scale, despite their being constructed from different samples. While the densities are all normalised such that the median of each distribution is unity, and the fitted trends are all quite similar, nevertheless there is a small scatter in the fitted trends. Here we describe an alternative test that relies only on the ranks of stars within their populations of neighbours, both in terms of phase space density and the residuals after detrending.

As each sample may contain a different number of stars, we first define fractional ranks between 0 and 1 such that

$$f_\rho = r_\rho / N_{\text{sample}} \quad (\text{A.1})$$

and

$$f_{\text{res}} = r_{\text{res}} / N_{\text{sample}}, \quad (\text{A.2})$$

where r_ρ and r_{res} are the ranks (1 being high) of each star in density and in the residuals, and N_{sample} is the number of stars in the sample. We now compare the Hot Jupiter hosts to the neighbours of the Sun. For each Hot Jupiter host, we calculate its fractional ranks, and pair it up with the nearest-ranked neighbour of the Sun, with rank (in density)

$$r_{\text{comp}} = \text{floor}(N_{\text{control}} f_{\rho, \text{HJ}}), \quad (\text{A.3})$$

where $N_{\text{control}} = 600$ is the number of neighbours of the Sun, and $f_{\rho, \text{HJ}}$ is the fractional density rank of the Hot Jupiter host. We then construct a control distribution of residuals by selecting the fractional residuals ranks of the Solar neighbours whose density ranks are given by r_{comp} .

This procedure is illustrated in Figure A.6. The fractional ranks for the Hot Jupiter hosts are shown in the left-hand panel. The density of points increases towards the bottom left. The increase towards the left reflects the tendency for Hot Jupiter hosts to have high phase space densities. The increase towards the bottom shows that they tend to have high residuals after detrending. However, even an unbiased sample can show a tendency for high density to correspond with high residuals. This is demonstrated in the middle panel of Figure A.6, where we show the equivalent rankings for the 600 neighbours of the Sun. In the right-hand panel of Figure A.6, we show the comparison between the Hot Jupiter sample and the control sample drawn from the centre panel. The Hot Jupiter sample and the control sample are then indistinguishable on a KS test ($p = 0.32$). Note that a set of randomly-selected neighbours of the Sun would give a uniform distribution.

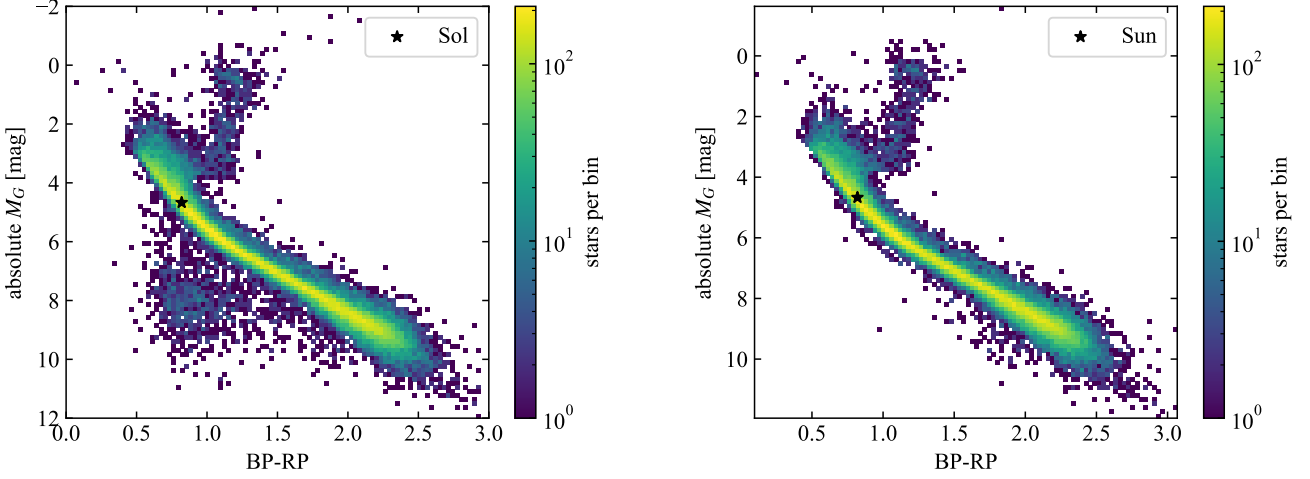


Fig. A.1. Colour–magnitude diagrams for all stars within 80 pc of the Sun with *Gaia* RVs. Left: DR2. Right: EDR3. The *Gaia* colour and magnitude for the Sun are taken from Casagrande & Vandenberg (2018).

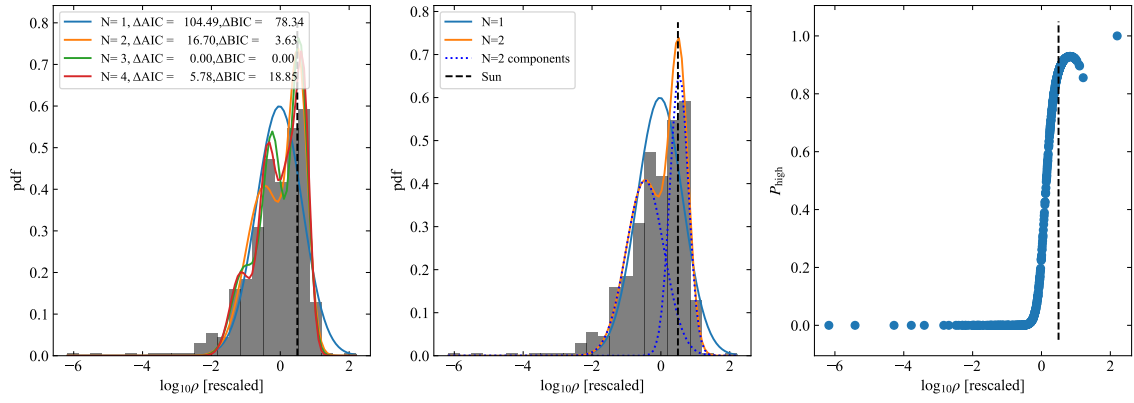


Fig. A.2. Gaussian Mixture models for the local phase space density of the Sun. Left: one- to ten-component models, together with Aikake and Bayesian Information criteria values relative to the best fit. Middle: The one- and two-component models, together with the decomposition of the latter. Right: probability each star belongs to the high-density component of the two-component model.

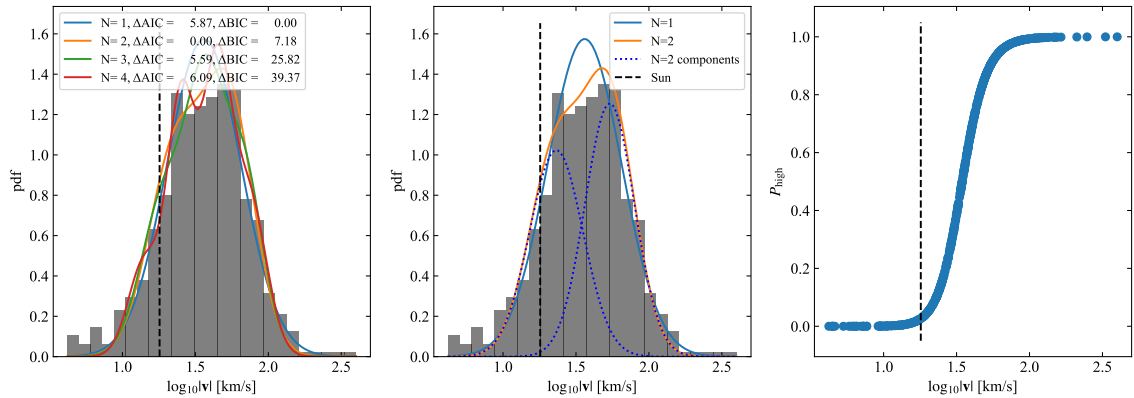


Fig. A.3. Gaussian Mixture models for the local peculiar velocity distribution of neighbours of the Sun. Left: one- to ten-component models, together with Aikake and Bayesian Information criteria values relative to the best fit. Middle: The one- and two-component models, together with the decomposition of the latter. Right: probability each star belongs to the high-velocity component of the two-component model.

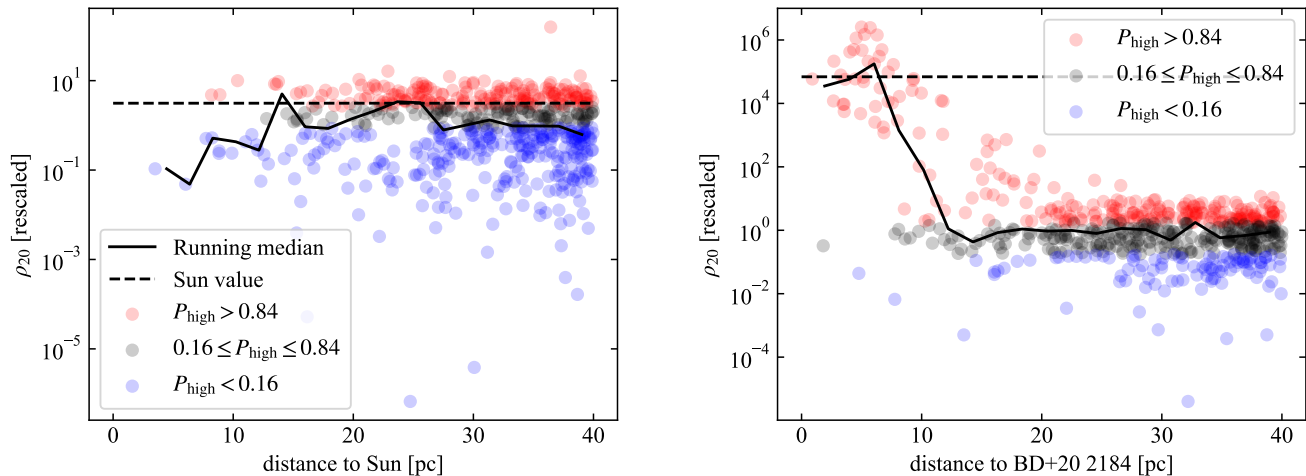


Fig. A.4. Local 20th-nearest neighbour phase space density, and probability of membership in the high-density population, for 600 stars within 40 pc of the Sun (left) and Pr0201 (BD+20 2184, right). We show these as a function of the distance to the target star.

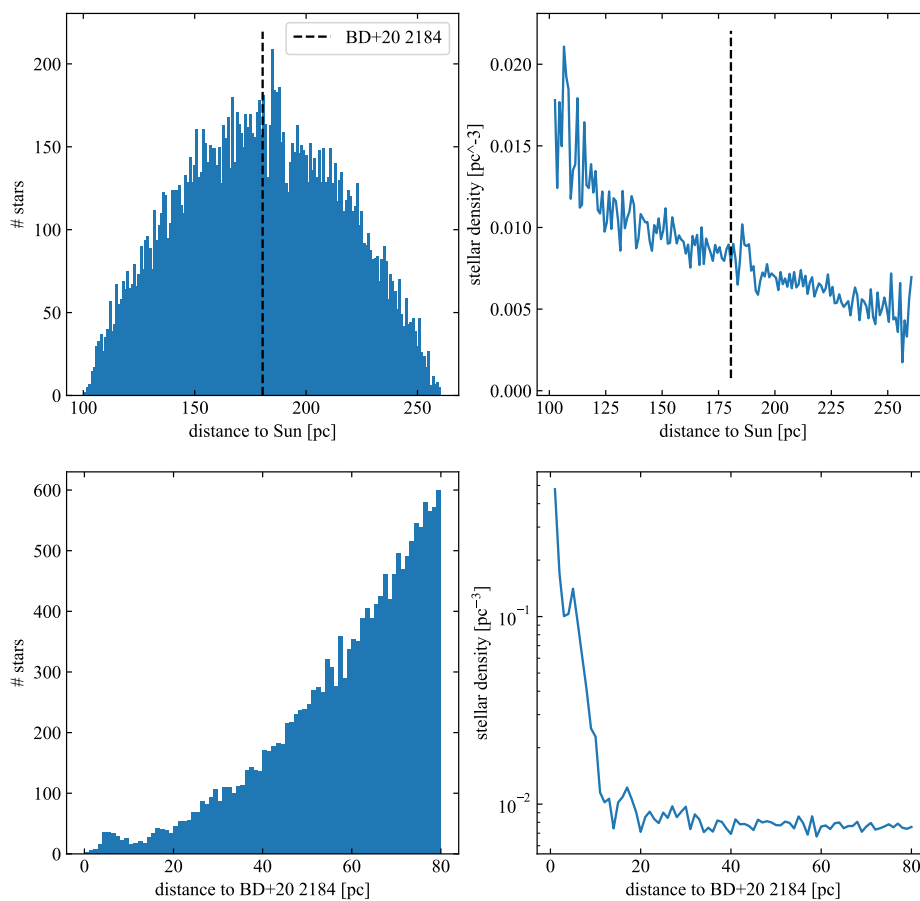


Fig. A.5. Differential completeness of the *Gaia* EDR3 RV catalogue across a sphere of 80 pc centred on BD+20 2184. Left-hand panels show histograms of the number of stars per distance bin, measured from the Sun (top) and from BD+20 2184 (bottom). Right-hand panels show the corresponding 3D spatial density.

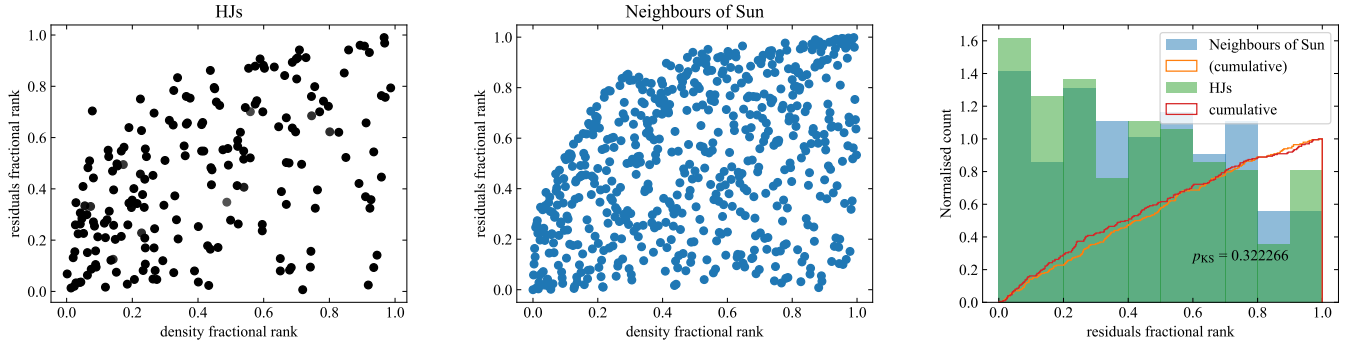


Fig. A.6. Left: The fractional rank (rank among neighbours divided by number of neighbours) in phase space density, and in residuals to the detrended phase space density, for all the 198 Hot Jupiter hosts. Darker symbols are stars with more neighbours in *Gaia* EDR3. Centre: The same, for 600 neighbours of the Sun. Right: The histogram of the fractional residuals rank for the Hot Jupiter hosts (blue for differential, orange for cumulative), and for the fractional residuals rank of 198 neighbours of the Sun chosen to have the same density fractional rank as the Hot Jupiter hosts (green for differential, red for cumulative). The KS test p -value comparing the two distributions is also displayed, showing that they are statistically indistinguishable.